American Mineralogist, Volume 75, pages 1282–1289, 1990

Formation of coexisting *1M* and *2M* polytypes in illite from an active hydrothermal system

Steven W. Lonker
Department of Geology, Australian National University, GPO Box 4, Canberra A.C.T. 2601, Australia
John D. Fitz Gerald
Research School of Earth Sciences, Australian National University, GPO Box 4, Canberra A.C.T. 2601, Australia

Abstract

Polytypes of illite from the Broadlands-Ohaaki geothermal system in New Zealand have been studied with transmission electron microscopy and electron diffraction. The illite is predominantly a one-layer polytype with 1.0-nm interlayer spacing. On the scale of a few millimeters, illite occurs as ordered crystals, disordered crystals, and crystals with regions of ordered and disordered stacking. Some crystals are composed entirely of either the one-layer or the two-layer polytype; others show regions of two-layer stacking in a one-layer host. Long period stacking sequences (3- or 4-layer) are less common and occur as lamellar intergrowths in *1M* mica. No morphological differences were observed among the discrete crystals of $1M_d$, *1M*, and *2M*. Textures indicate that regions with two-layer stacking can be produced from $1M_d$ mica even though there is a general trend with increasing temperature of $1M_d$ to *1M* to *2M*. Experimental data on the rate of transformation of *1M* to $2M_1$ muscovite combined with estimates of the mole fraction of *2M* mica and temperatures of illite crystallization were used to place constraints on the duration of hydrothermal activity in the Broadlands-Ohaaki system.

Introduction

Experimental, field, and theoretical studies have described the structural, compositional, and environmental factors that are responsible for polytypism in micas (see reviews in Baronnet, 1980; Środoń and Eberl, 1984; Frey, 1987). Yoder and Eugster (1955), Yoder (1959), and Velde (1965) found that the sequence of polytypic conversion was the sluggish reaction of $1M_d$ to *1M* to $2M_1$ with increasing hydrothermal experiment time, temperature, or pressure. This sequence is also promoted by the increasing H_2O-rock ratio (Mukhamet-Galeyev et al., 1985), decreasing disorder in the structure of the starting material (Velde, 1965; Mukhamet-Galeyev et al., 1985), or decreasing supersaturation (Baronnet, 1980; Amouric and Baronnet, 1983; Mukhamet-Galeyev et al., 1985). It became increasingly apparent from field and experimental studies that many polytypic structures do not have well-defined stability fields and that growth mechanisms and kinetics of polytypic transformations played the key role in the mode of stacking in micas (Baronnet, 1980). Several hypotheses have been proposed for the mechanism of polytypic transformation in micas: (1) layer-by-layer replacement (Takéuchi and Haga, 1971; Hunziker et al., 1986; Ballantyne, 1988) and (2) dissolution-recrystallization (Baronnet, 1980; Mukhamet-Galeyev et al., 1985; Inoue et al., 1988). Baronnet (1980) and Amouric and Baronnet (1983) have experimentally investigated nucleation and growth mechanisms in synthetic muscovite polytypes. They have observed nucleation of an initially dislocation-free basic structure that is *1M*-like or *2M*-like followed by layer-by-layer growth. The selection of the basic structure would be controlled by structural constraints imposed by the initial layer and environmental factors (i.e., nucleation temperature, degree of supersaturation). Layers with a more ordered stacking sequence would nucleate at similar T, P_{H_2O}, and degree of supersaturation on both sides of a disordered nucleus of 1, 2, or 3 layers. With decreasing supersaturation, progressively younger layers would have a more ordered stacking sequence, promoting the transition from $1M_d$ to *1M* to $2M_1$. Stacking faults were observed to form from side-by-side nucleation of *1M*-like and *2M*-like cores.

X-ray diffraction techniques (XRD) are not suitable for studying the disordered stacking arrangements that are present in low temperature micas. Transmission electron microscopy (TEM) and X-ray analytical electron microscopy (AEM) have been used to study the growth mechanisms, crystal morphology, and compositional changes during the *1M* to $2M_1$ polytypic transformation in hydrothermal experiments using synthetic muscovite (Amouric and Baronnet, 1983; Mukhamet-Galeyev et al., 1985) and in the isolated clay fraction from rocks of hydrothermal origin (Inoue et al., 1987, 1988). Inoue et al. (1987), however, determined the polytypes in the hydrothermal phyllosilicates by XRD. Moreover, hydrothermally synthesized micas have high free energies, and metastable phases probably form first (Baronnet, 1980).

High-resolution transmission electron microscope (HRTEM) images of $1M_d$ dioctahedral mica show inter-

0003–004X/90/1112–1282$02.00

growths of different stacking sequences (1, 2, and 3 layer) by structure imaging in small areas of large single crystals (Iijima and Buseck, 1978; Tomura et al., 1978). A related but simpler technique, lattice fringe imaging (Iijima and Buseck, 1978), has been used effectively for many TEM studies of fine-grained naturally occurring phyllosilicates. The coexistence of one-layer and two-layer stacking in dioctahedral micas has been identified in a range of geological settings (Page and Wenk, 1979; Lee et al., 1986). Little electron microscope work, however, has been carried out on the evolution of layer-stacking sequences in natural dioctahedral micas. Therefore, TEM, AEM, and SAED (selected area electron diffraction) were used to study polytype occurrences in illite from the Broadlands-Ohaaki geothermal system, New Zealand. This system is well suited for such an investigation, for Eslinger and Savin (1973) carried out an XRD study of the phyllosilicates in several wells and found a measurable amount of the $2M_1$ polytype in two samples from well 16 at measured temperatures above 200 °C. Moreover, the alteration mineral assemblage of the Broadlands-Ohaaki system is well characterized (Browne and Ellis, 1970; Lonker et al., 1990).

Samples and methods of study

The samples for this study came from wells 12, 13, and 35 (Table 1). These rocks consist of hydrothermally altered siliceous volcanics and pyroclastics. The sample from a depth of 1275–1276 m in well 12 is from a more permeable flow zone. All other samples are from less permeable rock units stratigraphically above or below the flow zones. These less permeable rock units have a higher f_{CO_2} and temperature and lower pH, f_{O_2}, and f_{S_2} than the flow zones (Lonker et al., 1990). Illite from well 12 is associated with a more recent alteration from cooler, slightly acidic, CO_2- and H_2-rich, steam-heated waters (Lonker et al., 1990). The measured temperatures in Table 1, which were taken after postdrilling stabilization, do not show the temperature changes between flow zones and less permeable rock units and should serve only as a crude guide to temperatures of illite crystallization.

Mineral analyses of illite were obtained by wavelength-dispersive X-ray analysis on a Camebax electron microprobe using an accelerating voltage of 15 kV, a beam current of 10 nA, and a defocused beam diameter of 12 μm. Data reduction was performed using a ZAF correction procedure. Recalculated illite formulae were carefully checked for evidence of any contamination from grains of other minerals inadvertently included in the broad microprobe beam and were rejected if the sum of the octahedral sites was less than 1.98 or greater than 2.02.

Areas of sample three millimeters in diameter were detached from the thin sections and ion-thinned by Ar beam bombardment. The ion-thinned samples were examined with a Philips EM430T analytical TEM. Lattice-fringe images of phyllosilicates in the Broadlands-Ohaaki specimens were obtained using (00*l*) reflections and interpreted following Iijima and Buseck (1978), Amouric et al. (1981), Amouric and Baronnet (1983), Veblen (1983a, 1983b), Spinnler et al. (1984), and Guthrie and Veblen (1989, 1990). All images were recorded in an underfocused condition, normally in the range of −80 to −200 nm, and thick regions of foils were found to yield the most informative images (Iijima and Buseck, 1978). A problem exists in the characterization of mica using lattice-fringe images in the TEM because direct bombardment by the electron beam immediately causes a mottled texture to develop, presumably due to strain contrast (Page, 1980) from some distributed defects that are sensitive to irradiation. This mottled texture has been used (Lee et al., 1985; Ahn and Peacor, 1986), along with lattice-fringe spacings and microbeam analysis, as a characteristic that distinguishes illite from other phyllosilicates in multiphase systems. The interlayer spacing measured for mottled crystals of mica remains constant. This is demonstrated by the preservation of the 2.0-nm lattice-fringe spacing in $2M_1$ muscovite from Broken Hill, New South Wales, even after the mottled texture had developed and had been modified by substantial migration and coalescence of the strain centers through electron irradiation (Fitz Gerald, unpublished data).

High-resolution images of large single crystals need to be taken with great care so that specimen thickness, crystal orientation, defocusing, contribution of diffracted beams other than (00*l*) reflections, etc. can be controlled or measured (Amouric et al., 1981; Veblen, 1983a, 1983b; Guthrie and Veblen, 1989, 1990; Veblen et al., 1990). Such images can in principle be interpreted in considerable detail (Cowley and Iijima, 1976; Veblen and Buseck, 1979; Buseck and Cowley, 1983). The imaging experi-

Table 1. Description of samples

Well	Depth (m)	*T* (°C)*	Secondary mineral assemblages**										
			Ab	Ap	Ant	Cal	Chl	Ep	Ill	Kfs	Py	Qtz	Ttn
12	1235–1236	275	X		X	X	X		X		X	X	X
	1275–1276	276	X		X	X	X		X	X	X	X	X
	1373–1374	278	X	X	X	X	X		X			X	X
13	1038–1039	278	X		X	X	X	X	X	X	X	X	X
35	1374–1375	300					X	X	X	X		X	X

* Initial measured temperature after postdrilling stabilization (Ministry of Works and Development, 1977).

** Mineral abbreviations: Ab = albite; Ap = apatite; Ant = anatase; Cal = calcite; Chl = chlorite; Ep = epidote; Ill = illite; Kfs = potassium feldspar; Py = pyrite; Qtz = quartz; Ttn = titanite.

TABLE 2. Representative analyses of illite

	79	313	358	737	1081
SiO_2	48.26	48.80	49.44	50.27	49.44
Al_2O_3	33.64	31.64	32.04	32.36	34.43
TiO_2	0.00	0.00	0.00	0.00	0.20
FeO_{tot}	1.66	1.88	1.23	1.51	1.63
MnO	0.00	0.00	0.00	0.00	0.00
MgO	0.28	1.19	0.64	0.90	0.26
CaO	0.00	0.25	0.00	0.00	0.08
Na_2O	0.00	0.32	0.36	0.00	0.12
K_2O	10.56	10.42	9.20	9.76	9.72
Total	94.40	94.50	92.91	94.80	95.88
Formulae based on 11 O atoms					
Si	3.2263	3.2713	3.3217	3.3197	3.2328
Al	0.7737	0.7287	0.6783	0.6803	0.7672
Al	1.8772	1.7707	1.8588	1.8383	1.8856
Ti	0.0000	0.0000	0.0000	0.0000	0.0096
Fe	0.0926	0.1054	0.0691	0.0834	0.0889
Mn	0.0000	0.0000	0.0000	0.0000	0.0000
Mg	0.0283	0.1186	0.0641	0.0884	0.0250
$^{[6]}\Sigma$	1.9981	1.9947	1.9920	2.0101	2.0091
Ca	0.0000	0.0179	0.0000	0.0000	0.0059
Na	0.0000	0.0413	0.0469	0.0000	0.0157
K	0.9004	0.8912	0.7885	0.8217	0.8104
$^{[12]}\Sigma$	0.9004	0.9504	0.8354	0.8217	0.8320

Note: Sample numbers: 79 (well 35, 1374–1375 m, area 3); 313 (well 12, 1235–1236 m, sample B, area 3); 358 (well 13, 1038–1039 m, sample A, area 5); 737 (well 12, 1275–1276 m, sample C, area 4); 1081 (well 12, 1373–1374 m, sample A, area 1).

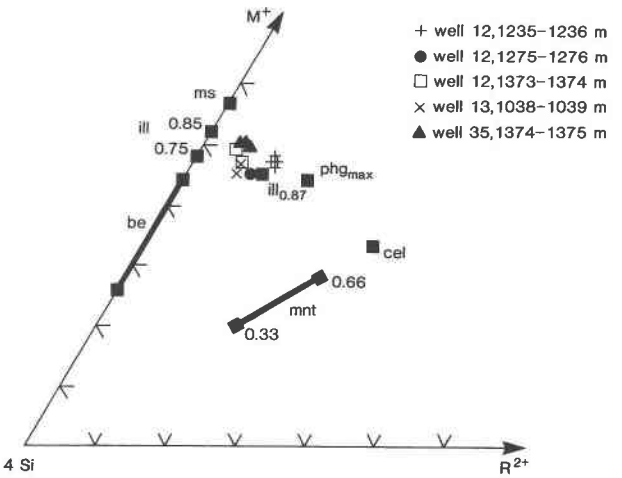

Fig. 1. Compositions of illite samples plotted on a diagram of M^+-4Si-R^{2+} after Meunier and Velde (1989). Abbreviations are be = beidellite, cel = celadonite, ill = illite, mnt = montmorillonite, ms = muscovite, and phg_{max} = maximum phengite substitution. M^+ is the layer charge, 4Si is the maximum Si content of the tetrahedral sheet, and R^{2+} is the total number of divalent cations in the octahedral site. Layer charges per $O_{10}(OH)_2$ are given by the numbers (0.33, 0.66, 0.75, 0.85, 0.87). Meunier and Velde (1989) and references therein list coordinates of the phyllosilicates in the M^+-4Si-R^{2+} system.

ments, however, are poorly controlled in fine-grained materials such as those from the Broadlands-Ohaaki system. Only mats of thin, subparallel crystals can be aligned with a strong (00*l*) reflection averaged over a group of crystals. Little control can be exercised with regard to the exact direction of the incident electron beam relative to the local crystallographic axes of individual grains, so one critical requirement for formation of an interpretable image (Iijima and Buseck, 1978) cannot be fulfilled. The grain orientations will certainly have planes (00*l*) nearly parallel to the electron beam, but the relationship between electron beam direction and [*hk*0] is expected to be random overall. Such poor control over [*hk*0] orientation will have consequences even for (00*l*) lattice-fringe imaging, since many crystal orientations may produce good (00*l*) lattice fringes but not yield polytype information. Selected-area electron diffraction patterns could not be obtained from many of the single crystals because of the small grain size. The absolute value of the lattice parameters determined from the SAED patterns is estimated to have a 1% uncertainty, which is insufficient to determine the changes in the *b* parameter with interlayer content as described by Meunier and Velde (1989). Also, many grains in the ion-thinned Broadlands-Ohaaki materials appear to be weakly distorted, so the image contrast can be expected to vary across individual crystals.

Mineral chemistry

The occurrence and composition of illite in the Broadlands-Ohaaki system are described in detail by Lonker et al. (1990) and are therefore only briefly discussed here. Representative analyses are given in Table 2. Figure 1 is a diagram for M^+-4Si-R^{2+} from Meunier and Velde (1989) showing the compositions of the analyzed illite samples. The illite compositions lie outside of the illite-montmorillonite field and are distributed along the line from beidellitic $illite_{0.85}$ to phengitic $illite_{0.87}$. Meunier and Velde (1989) suggested that the line from beidellitic $illite_{0.85}$ to phengitic $illite_{0.87}$ defines the boundary between the *1M* and $2M_1$ polytype domains. The $2M_1$ polytype compositions would fall on the K-rich side of this line.

Electron diffraction and TEM images

The illite occurs as well-formed crystals in porous aggregates (Fig. 2a). Pores between illite grains were carefully examined with microbeam AEM, but no infilling phases could be detected. This is an important result for interpretation of the analytical results, because full confidence can then be placed in the broad-beam electron microprobe analyses. For the illite, fine grain size and stacking disorder make it difficult to detect minor compositional changes with AEM, as well as to conduct tilting experiments in order to enhance the periodicity due to polytypism in lattice-fringe images and to observe stacking in more than one zone of the same area in a crystal. No intergrown smectite with its characteristic wavy, discontinuous, and distorted layers (Yau et al., 1987) was observed, and the analyzed compositions of the illite (Fig. 1) argue against illite-smectite intergrowth at the unit-cell scale. Intergrowths of illite with chlorite are uncommon (Lonker et al., 1990). Turbostratic stacking, which is common in many clay minerals, was not observed in the SAED patterns of larger grains. The illite is predomi-

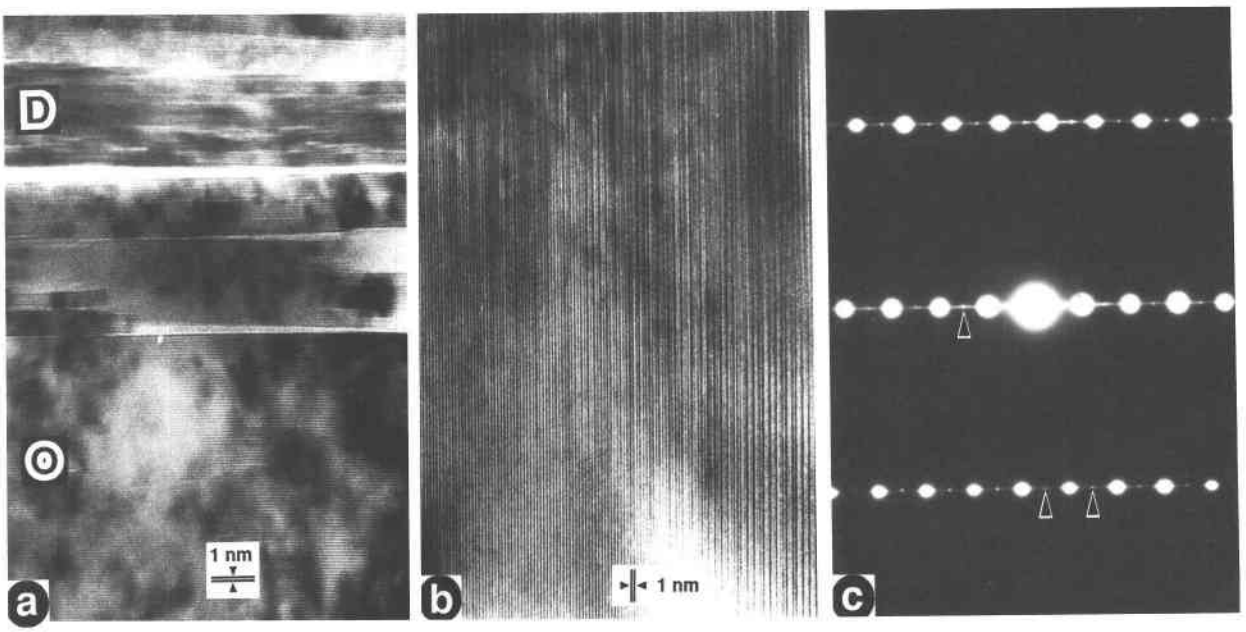

Fig. 2. (a) Transmitted electron image showing well-formed crystals of ordered (O) *1M* illite as well as illite crystals with disordered (D) stacking arrangements from well 12, depth of 1235–1236 m. (b) The (00*l*) lattice-fringe image of relatively coarse-grained illite showing stacking disorder from well 12, depth of 1373–1374 m. The visibility of polytypic layering is variable, probably because of local variations in thickness and orientation. (c) Selected-area electron diffraction pattern of illite from well 35, depth of 1374–1375 m, showing streaking along c* caused by stacking disorder and diffraction spots due to a small amount of *2M*. Arrows point to several of the 2.0-nm diffraction spots.

nantly a one-layer polytype with straight, continuous (00*l*) fringes, $d_{(001)} = 1.0$ nm, and varying degrees of stacking disorder as indicated by streaking along c* in the SAED patterns (Figs. 2b, 2c). Discrete crystals show ordered one-layer stacking, disordered one-layer stacking, or regions of both ordered and disordered stacking (Fig. 2a).

Two-layer stacking sequences ($2M_1$ or $2M_2$) can be found in individual samples as regions of *2M* layering in the *1M* host (Fig. 3a), as discrete crystals (Figs. 3b, 3c), and as distorted crystals (Fig. 3d). No attempt was made to record zone axis patterns that could have been used to delineate between the $2M_1$ and $2M_2$ polytypes. Some of the local variations in stacking sequence in the images across a single crystal may be due to differences in orientation (Figs. 3c, 3d). Two-layer stacking is more common in the higher temperature sample from well 35, 1374–1375 m. No relationship was observed between one-layer stacking order and the presence of regions of two-layer stacking. The morphology of the discrete crystals of *2M* appears to be the same as that of the *1M* crystals (Figs. 2b, 3c). It was not possible to study the morphology as a function of crystallographic orientation in these small crystals. The two-layer lamellae have a crystallographically controlled orientation, and the interfaces of one-layer with two-layer lamellae do not show grain boundary gaps or appreciable strain contrast (Fig. 3a). In the other intergrowths, there are grain boundary gaps between crystals with different polytypic stacking sequences, or the nature of the grain boundary is indeterminate.

Long-period stacking sequences are less common. Three- and four-layer polytypes occur as lamellar intergrowths within the one-layer host (Fig. 4). The grain boundaries between these long-period stacking sequences and the one-layer host appear to be sharp with little strain contrast (Fig. 4).

Duration of hydrothermal activity

Experimental data from Mukhamet-Galeyev et al. (1985) regarding the kinetics of the transformation from *1M* to $2M_1$ muscovite can be used to place semiquantitative constraints on the duration of hydrothermal activity. This polytypic transformation is slow below 450–500 °C, so experiments have been conducted at 600–700 °C and 600–700 MPa in the presence of a fluid phase and extrapolated to lower temperatures. Figure 5 is a plot of $\ln[1M/(1M + 2M_1)]$ vs. time and shows that the polytypic conversion rate is nearly linear at 650 and 700 °C. Thus, the overall rate of polytypic transformation at these temperatures can be defined by a first-order rate law. The experimental data at 600 °C were not always reproducible, and the data may indicate that at least two processes (nucleation and growth) limited the rate of polytypic transformation (Mukhamet-Galeyev et al., 1985). The 600 °C data, however, in a first approximation fit a linear curve yielding an activation energy that is nearly constant from 600 to 700 °C.

The experimental data depicted in Figure 5 fit the first-order rate law

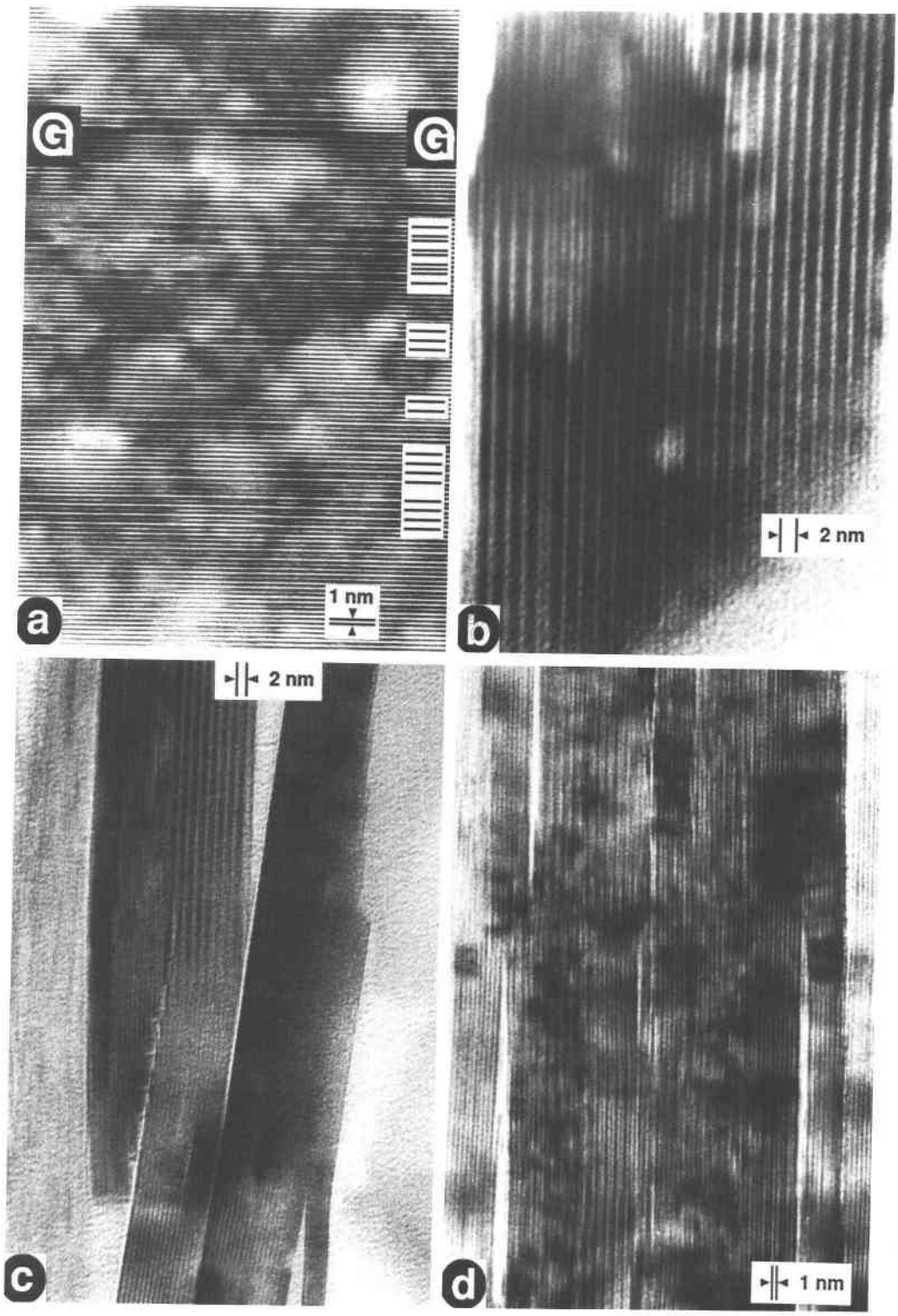

Fig. 3. (**a**) The (00*l*) lattice-fringe image of illite from well 12, depth of 1373–1374 m, showing lamellae of *2M* in $1M_d$ with the grain boundary running from G to G. The horizontal lines delineate possible one- and two-layer stacking sequences, which can best be viewed at a low angle from the side of the photograph. (**b**) The (00*l*) lattice-fringe image showing well-ordered *2M* layering from well 12, depth of 1373–1374 m. (**c**) Transmitted electron image showing a kinked crystal with *2M* layering at one end and $1M_d$ at the other end of the crystal from well 12, depth of 1235–1236 m. Differences in stacking sequences across a single crystal in the images may be due to orientation. Discrete crystals of *1M* and $1M_d$ are also present. (**d**) Transmitted electron image showing a distorted crystal consisting mainly of *2M* and a smaller amount of $1M_d$ from well 35, depth of 1374–1375 m. Local variations in stacking sequence may be due to differences in orientation and thickness. The origin of the lens-shaped regions of low mass density is indeterminate.

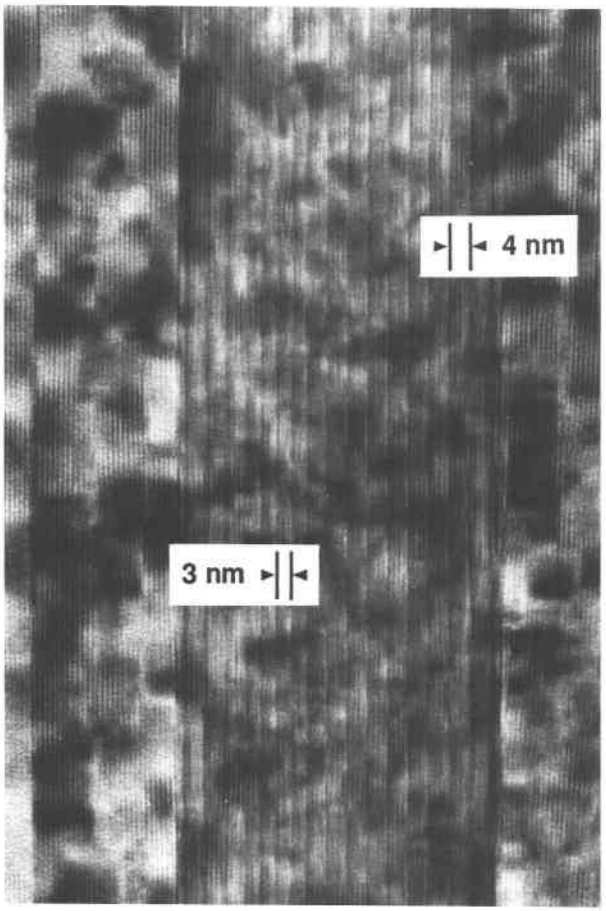

Fig. 4. The (00*l*) lattice-fringe image of illite showing ordered regions of three- and four-layer periodicity in $1M_d$ from well 12, depth of 1235–1236 m.

$$\ln X_{1M} = \ln X^0_{1M} - kt \quad (1)$$

where $X_{1M} = 1M/(1M + 2M_1)$, k = rate constant (s^{-1}), and t = time (s). Table 3 gives the rate constants and correlation coefficients extracted from the linear regression of $\ln X_{1M}$ vs. t at constant temperature using the data depicted in Figure 5. Figure 6 is a plot of $\ln k$ vs. $1/T$. The rate constants in Figure 6 fit the equation

$$\ln k = -E_a/\mathrm{R}(1/T) + \ln \mathrm{A}(T) \quad (2)$$

where T = temperature (K) and R = 8.31451 J/mol K, yielding a preexponential factor [ln A(T)] of 15.298 and an activation energy (E_a) of 216 kJ/mol, which can be compared with the estimate of 213 ± 42 kJ/mol by Mukhamet-Galeyev et al. (1985). The pressure correction ($P\Delta V/\mathrm{R}T$) is small ($\Delta V^0_{298.15} = -1.261$ J/MPa, Blencoe, 1977).

TABLE 3. Rate constants and correlation coefficients

T(°C)	P(MPa)	k(s^{-1})	r
700	700	1.1249E-5	0.996
650	700	2.8881E-6	0.992
600	600	5.3232E-7	0.974

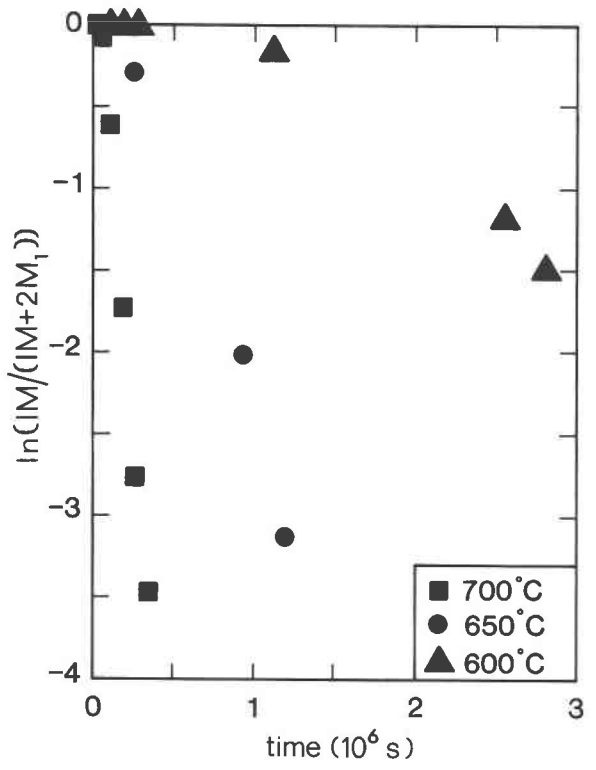

Fig. 5. Experimental data of Mukhamet-Galeyev et al. (1985) plotted as a function of $\ln[1M/(1M + 2M_1)]$ and time (10^6 s) at 600, 650, and 700 °C.

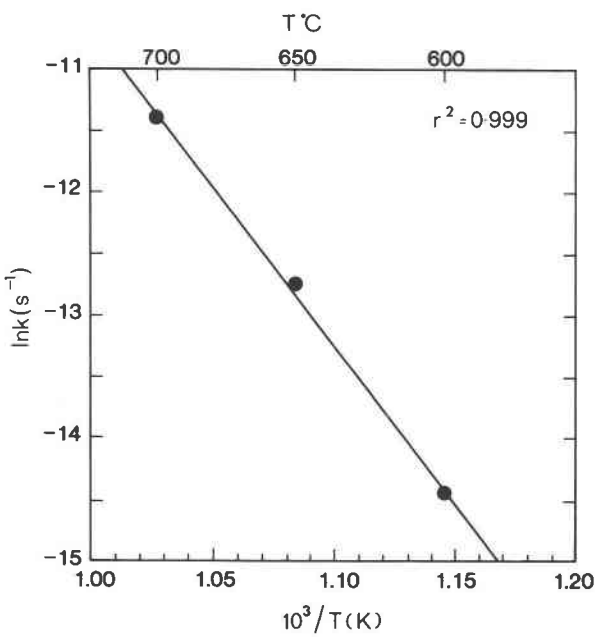

Fig. 6. Plot of $\ln k$ (s^{-1}) vs. $10^3/T$ (K). The slope of line is E_a/R, where E_a is the activation energy and R is the universal gas constant.

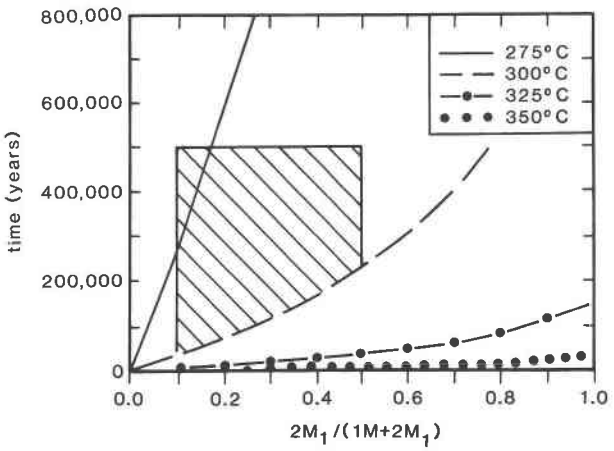

Fig. 7. Time (yr) vs. $2M_1/(1M + 2M_1)$ with contours of temperature. Hachured area shows the time it would take to form between 10% and 50% $2M_1$ in the studied samples from the Broadlands-Ohaaki geothermal system. The upper limit of the hachured area is the maximum estimate for the duration of thermal activity in the Broadlands-Ohaaki system (Weissberg et al., 1979).

The estimates of the activation energy and the preexponential factor were used to calculate X_{2M_1} as a function of temperature and time using Equations 1 and 2 (Fig. 7). It was assumed that there were no $2M_1$ nuclei formed during the initial induction period, which corresponds to the time elapsed between the creation of the supersaturated state and the appearance of $2M_1$. The TEM observations indicate that 10–50% of the illite in the studied samples is *2M* (?$2M_1$). The measured well temperatures place crude constraints on the temperature of crystallization of illite in the studied samples between 270 and 300 °C. Figure 7 shows that it would take more than 35000 years to form 10% $2M_1$ and more than 230000 years to form 50% $2M_1$. Weissberg et al. (1979) placed the duration of thermal activity in the Broadlands-Ohaaki system between 150000 and 500000 years (upper limit in Fig. 7).

Discussion

It is difficult to determine the mechanism of polytypic transformation from textures alone, particularly since there is so much textural variation on the scale of a few millimeters. Lamellar intergrowths of two or more polytypes may be due to any of the following: (1) solid state replacement by a structural rearrangement due to introduction of stacking faults or microtwinning; (2) simultaneous nucleation from solution of *1M* and *2M* grains followed by coalescence by growth (Baronnet, 1980; Amouric and Baronnet, 1983); or (3) dissolution of *1M* and later precipitation from the solution of narrow nuclei of *2M* and larger periodicity stacking sequences within *1M*. The absence of relict lamellae of *1M* in *2M* or larger periodicity sequences indicate that any replacement reaction went to completion. Well-formed discrete crystals of *2M*, which occur in pore spaces and contain no remnants of *1M*, either crystallized directly from solution or represent complete replacement. Dissolution and precipitation would probably involve a compositional change, but this would probably be too subtle to detect using AEM in small grains, because of beam damage and volatilization problems (Mackinnon and Kaser, 1987).

Conclusions

The results of this investigation show the complex nature of coexisting polytypes in a natural system. A solid-state transformation mechanism (Takéuchi and Haga, 1971; Hunziker et al., 1986; Ballantyne, 1988) cannot be ruled out for the origin of lamellae of *2M* and higher periodicity in a *1M* host in the Broadlands-Ohaaki illite. There is not enough information to prove that the fringe-spacing sequence in the studied samples formed from layer-by-layer growth of symmetrically positioned layers with a higher degree of order around a disordered core or that a faulted matrix was produced by side-by-side nucleation and coalescence of *1M*-like and *2M*-like cores (Baronnet, 1980; Amouric and Baronnet, 1983). Although the overall trend with increasing temperature in the Broadlands-Ohaaki samples is the sequence of $1M_d$ to *1M* to *2M* (?$2M_1$), evidence has been presented that might suggest transformation of $1M_d$ directly to *2M* (?$2M_1$). The disordered *1M* mica crystals contain small regions only one or two unit cells wide with two-layer and larger periodicities. It is not possible to state with certainty what the stacking sequence of a short sequence of fringes actually is from such an image "where the contrast is embedded in a sea of disorder" (D. R. Veblen, personal communication, 1990). Although there is a coarsening of grain size in the illite sampled from the highest measured temperatures in the Broadlands-Ohaaki system (Lonker et al., 1990), no morphological changes were observed between discrete crystals of *1M* and *2M* mica. These crystals probably have random crystallographic orientations, and the absence of any observable changes in morphology may indicate little difference in interlayer content among the polytypes in the studied samples. Previous studies described morphological and compositional changes during the polytypic transformation (Mukhamet-Galeyev et al., 1985; Inoue et al., 1987, 1988; Meunier and Velde, 1989). There is no compositional or morphological evidence in the Broadlands-Ohaaki samples that the *1M* and *2M* micas are crystallographically distinct phases separated by a miscibility gap, as proposed by Meunier and Velde (1989).

Our estimates for the duration of hydrothermal activity from the rate of polytypic transformation are approximate. A rigorous quantitative analysis is not possible at this time because of the complexities of polytypic transformation in natural illite, the uncertainties in the temperatures of illite crystallization, the difficulties of extrapolating high temperature data to low temperatures and extrapolating pure synthetic end-member compositions to solid solutions with varying degrees of stacking and cation order, and the dependence of transformation rate on additional factors like H_2O-rock ratio, crystallization of $2M_1$ during the initial induction period, and the degree of supersaturation and composition of the solution. There

is a clear need for further TEM, SAED, and AEM studies on polytypic transformations and growth mechanisms in dioctahedral mica from other hydrothermal systems, as well as from relatively closed systems during diagenesis and low-grade metamorphism. Such information would be extremely useful if the rate of polytypic transformation, grain size, crystal morphology, and mica composition are to be used to place constraints on the duration, temperature, and fluid-rock ratios during hydrothermal activity, diagenesis, and low-grade metamorphism.

Acknowledgments

The research conducted by the senior author was supported by a National Research Fellowhip, J.L. Walshe, Senior Investigator. The authors wish to thank the Chemistry Division of the Department of Scientific and Industrial Research, New Zealand, for providing the samples and logs. Special thanks are due to Nick Ware for assisting in electron microprobe analysis, Robin Wescott for impregnation and polishing of thin sections, and Chris Foudoulis for preparation of ion-thinned samples for transmission electron microscopy. We wish to thank D.D. Eberl, R.A. Eggleton, and D.R. Veblen for their comments on the manuscript.

References cited

Ahn, J.H., and Peacor, D.R. (1986) Transmission and analytical electron microscopy of the smectite-to-illite transition. Clays and Clay Minerals, 34, 165–179.

Amouric, M., and Baronnet, A. (1983) Effect of early nucleation conditions on synthetic muscovite polytypism as seen by high resolution transmission electron microscopy. Contributions to Mineralogy and Petrology, 9, 146–159.

Amouric, M., Mercuriot, G., and Baronnet, A. (1981) On computed and observed HRTEM images of perfect mica polytypes. Bulletin de Minéralogie, 104, 298–313.

Ballantyne, J.M. (1988) A sheet zipper theory of illitization: Implications and evidence. Geological Society of America Abstracts with Programs, 20, 357.

Baronnet, A. (1980) Polytypism in micas: A survey with emphasis on the crystal growth aspect. In E. Kaldis, Ed., Current topics in materials science, 5, p. 447–548. North Holland, Amsterdam.

Blencoe, J.G. (1977) Molal volumes of synthetic paragonite-muscovite micas. American Mineralogist, 62, 1200–1215.

Browne, P.R.L., and Ellis, A.J. (1970) The Ohaki-Broadlands hydrothermal area, New Zealand: Mineralogy and related geochemistry. American Journal of Science, 269, 97–131.

Buseck, P.R., and Cowley, J.M. (1983) Modulated and intergrowth structures in minerals and electron microscopic methods for their study. American Mineralogist, 68, 18–40.

Cowley, J.M., and Iijima, S. (1976) The direct imaging of crystal structures. In H.-R. Wenk, Ed., Electron microscopy in mineralogy, p. 123–136. Springer-Verlag, Berlin.

Eslinger, E.V., and Savin, S.M. (1973) Mineralogy and oxygen isotope geochemistry of hydrothermally altered rocks of the Ohaki-Broadlands, New Zealand geothermal area. American Journal of Science, 273, 240–267.

Frey, M. (1987) Very low-grade metamorphism of clastic sedimentary rocks. In M. Frey, Ed., Low temperature metamorphism, p. 9–58. Blackie, Glasgow.

Guthrie, G.D., Jr., and Veblen, D.R. (1989) High-resolution transmission electron microscopy of mixed-layer illite/smecite: Computer simulations. Clays and Clay Minerals, 37, 1–11.

——— (1990) Interpreting one-dimensional high-resolution transmission electron micrographs of sheet silicates by computer simulation. American Mineralogist, 75, 276–288.

Hunziker, J.C., Frey, M., Clauer, N., Dallmeyer, R.D., Friedrichsen, H., Flehmig, W., Hochstrasser, K., Roggwiler, P., and Schwander, H. (1986) The evolution of illite to muscovite: Mineralogical and isotopic data from the Glarus Alps, Switzerland. Contributions to Mineralogy and Petrology, 92, 157–180.

Iijima, S., and Buseck, P.R. (1978) Experimental study of disordered mica structures by high-resolution electron microscopy. Acta Crystallographica, A34, 709–719.

Inoue, A., Kohyama, N., Kitagawa, R., and Watanabe, T. (1987) Chemical and morphological evidence for the conversion of smectite to illite. Clays and Clay Minerals, 35, 111–120.

Inoue, A., Velde, B., Meunier, A., and Touchard, G. (1988) Mechanism of illite formation during smectite-to-illite conversion in a hydrothermal system. American Mineralogist, 73, 1325–1334.

Lee, J.H., Ahn, J.H., and Peacor, D.R. (1985) Textures in layered silicates: Progressive changes through diagenesis and low-temperature metamorphism. Journal of Sedimentary Petrology, 55, 532–540.

Lee, J.H., Peacor, D.R., Lewis, D.D., and Wintsch, R.P. (1986) Evidence for syntectonic crystallization for the mudstone to slate transition at Lehigh Gap, Pennsylvania, U.S.A. Journal of Structural Geology, 8, 767–780.

Lonker, S.W., Fitz Gerald, J.D., Hedenquist, J.W., and Walshe, J.L. (1990) Mineral-fluid interactions in the Broadlands-Ohaaki geothermal system, New Zealand. American Journal of Science, 290, 995–1068.

Mackinnon, I.D.R., and Kaser, S.A. (1987) Microanalysis of clays at low temperature. In R.H. Geiss, Ed., Microbeam analysis—1987, p. 332–334. San Francisco Press, San Francisco.

Meunier, A., and Velde, B. (1989) Solid solutions in I/S mixed-layer minerals and illite. American Mineralogist, 74, 1106–1112.

Ministry of Works and Development (1977) Broadlands geothermal field investigation report. Wellington, 234 p.

Mukhamet-Galeyev, A.P., Pokrovskiy, V.A., Zotov, A.V., Ivanov, I.P., and Samotoin, N.D. (1985) Kinetics and mechanism of hydrothermal crystallization of $2M_1$ muscovite: An experimental study. International Geology Review, 27, 1357–1364.

Page, R.H. (1980) Partial interlayers in phyllosilicates studied by transmission electron microscopy. Contributions to Mineralogy and Petrology, 75, 309–314.

Page, R.H., and Wenk, H.-R. (1979) Phyllosilicate alteration of plagioclase studied by transmission electron microscopy. Geology, 7, 393–397.

Spinnler, G.E., Self, P.G., Iijima, S., and Buseck, P.R. (1984) Stacking disorder in clinochlore chlorite. American Mineralogist, 69, 252–263.

Środoń, J., and Eberl, D.D. (1984) Illite. In S.W. Bailey, Ed., Micas, Mineralogical Society of America Reviews in Mineralogy, 13, 495–544.

Takéuchi, Y., and Haga, N. (1971) Structural transformation of trioctahedral sheet silicates: Slip mechanisms of octahedral sheets and polytypic changes of micas. Mineralogical Society of Japan Special Paper 1, 74–87.

Tomura, S., Kitamura, M., and Sunagawa, I. (1978) High resolution electron microscopy of dioctahedral mica. Mineralogical Magazine, 9, 129–136.

Veblen, D.R. (1983a) Exsolution and crystal chemistry of the sodium mica wonesite. American Mineralogist, 68, 554–565.

Veblen, D.R. (1983b) Microstructures and mixed layering in intergrown wonesite, chlorite, talc, biotite, and kaolinite. American Mineralogist, 68, 566–580.

Veblen, D.R., and Buseck, P.R. (1979) Chain-width order and disorder in biopyriboles. American Mineralogist, 64, 687–700.

Veblen, D.R., Guthrie, G.D., Jr., and Livi, K.J.T. (1990) High-resolution transmission electron microscopy and electron diffraction of mixed-layer illite/smectite: Experimental results. Clays and Clay Minerals, 38, 1–13.

Velde, B. (1965) Experimental determination of muscovite polymorph stabilities. American Mineralogist, 50, 436–449.

Weissberg, B.G., Browne, P.R.L., and Seward, T.M. (1979) Ore metals in active geothermal systems. In H.L. Barnes, Ed., Geochemistry of hydrothermal ore deposits, p. 738–780. Wiley, New York.

Yau, Y.C., Peacor, D.R., and McDowell, S.D. (1987) Smectite-to-illite reactions in Salton Sea shales: A transmission and analytical electron microscopy study. Journal of Sedimentary Petrology, 57, 335–342.

Yoder, H. S. (1959) Experimental studies on micas: A synthesis. Clays and Clay Minerals, 6, 42–60.

Yoder, H.S., and Eugster, H.P. (1955) Synthetic and natural muscovites. Geochimica et Cosmochimica Acta, 8, 225–280.

Manuscript received January 6, 1990
Manuscript accepted October 2, 1990